in silico Plants, 2022, **5**, 1–12
https://doi.org/10.1093/insilicoplants/diac022
Advance access publication 26 December 2022
SPECIAL ISSUE: Multiscale Modelling of Photosynthesis

in silico Plants

OXFORD

SPECIAL ISSUE: Multiscale Modelling of Photosynthesis Original Research

The trade-off function of photorespiration in a changing environment

Jakob Sebastian Hernandez and Thomas Nägele*

Ludwig-Maximilians-Universität München, Faculty of Biology, Plant Evolutionary Cell Biology, Großhaderner Str. 2-4, 82152 Planegg, Germany

*Corresponding author's e-mail address: thomas.naegele@lmu.de

Citation: Hernandez JS, Nägele T. 2022. The trade-off function of photorespiration in a changing environment. *In Silico Plants* 2022: diac022; doi: 10.1093/insilicoplants/diac022

Handling Editor: Xin-Guang Zhu

ABSTRACT

The photorespiratory pathway in plants comprises metabolic reactions distributed across several cellular compartments. It emerges from the dual catalytic function of Rubisco, i.e. ribulose-1,5-bisphosphate carboxylase/oxygenase. Rubisco either carboxylates or oxygenates ribulose-1,5-bisphosphate. Carboxylation reactions produce 3-phosphoglycerate molecules which are substrates for the central carbohydrate metabolism. However, oxygenation reactions additionally form 2-phosphoglycolate molecules which are (i) substrate for a multicompartmental recovery process, and (ii) inhibit several enzymes of the Calvin–Benson–Bassham cycle. Here, an approach of structural kinetic modelling is presented to investigate the extent of stabilization of the Calvin–Benson–Bassham cycle and carbohydrate metabolism by photorespiration. This method is based on a parametric representation of the Jacobian matrix of a metabolic system which offers a robust strategy for handling uncertainties associated with *in vitro* kinetic constants. Our findings indicate that oxygenation of ribulose-1,5-bisphosphate by Rubisco significantly stabilizes the Calvin–Benson–Bassham cycle. Hence, a trade-off function of photorespiration is suggested which reduces carbon assimilation rates but simultaneously stabilizes metabolism by increasing plasticity of metabolic regulation within the chloroplast. Furthermore, our analysis indicates that increasing carbon flux towards sucrose biosynthesis has a stabilizing effect. Finally, our findings shed light on the role of a multicompartmental metabolic pathway in stabilizing plant metabolism against perturbation induced by a dynamic environment.

KEYWORDS: Photorespiration; photosynthesis; plant metabolism; stability; structural kinetic modelling.

1. INTRODUCTION

Cellular metabolism consists of a highly elaborate reaction network which frequently shows complex and non-intuitive dynamical behaviour. This behaviour can be deterministically described by a system of ordinary differential equations, ODEs (Klipp *et al.* 2016). Such a kinetic model can then be used to analyse and simulate consequences of environmental fluctuations, e.g. sudden changes of temperature or light intensity. These perturbations might result in a deviation of the metabolic system from its steady state. The system can then either return to its original state again (stable), exponentially diverge from its original state (unstable) or be metastable (behaviour is indifferent). The formulation of ODEs in a kinetic model is, however, typically challenged by lacking experimental data on enzymatic parameters, which are often laborious and difficult to quantify (Wittig *et al.* 2014). Furthermore, enzymatic activity *in vivo* depends on numerous factors, such as temperature and pH, thus greatly increasing the permissive parameter space which exacerbates the physiological interpretation of *in vitro* data (Bisswanger 2017).

Previously, the approach of structural kinetic modelling (SKM) was developed which allows for quantitative evaluation of dynamic properties without referring to any explicit system of ODEs, and which is achieved by a parametric representation of the Jacobian matrix (Steuer *et al.* 2006). Structural kinetic modelling has been confirmed to be a suitable approach for evaluation of the stability and robustness of metabolic states (Grimbs *et al.* 2007). It has been successfully used in a variety of studies

to analyse metabolism and its regulation (Grimbs *et al.* 2007; Reznik and Segrè 2010; Fürtauer and Nägele 2016). However, evaluation of regulatory interactions between a metabolite and reaction of interest is complicated by the complex interplay found within the highly dynamic system of cellular metabolism. Depending on the regulatory setting, a single regulatory interaction can be beneficial or detrimental for the system stability. Further, although a vast amount of data and information is available on regulatory interplay between genes, proteins and metabolites, e.g., provided by genome-scale metabolic networks (Tang *et al.* 2021), many regulatory and metabolic interactions can be assumed to remain elusive or unknown.

Carbon fixation takes place in the stroma of chloroplasts and is catalysed by the enzyme ribulose-1,5-bisphosphate carboxylase/oxygenase (Rubisco). This enzyme facilitates the carboxylation of ribulose-1,5-bisphosphate (RuBP) and subsequent cleavage between the C_2 and C_3 carbon forming two molecules of 3-phospho-D-glycerate (3-PGA) (Andersson 2008). In succeeding steps, 3-PGA is used in the Calvin-Benson-Bassham Cycle (CBBC) to resynthesize RuBP and supply the cell with triose phosphates which are substrate for starch and sucrose biosynthesis (Bassham *et al.* 1954; Martin *et al.* 2000). As the CBBC is directly connected to the rate of carbon fixation, its regulation is crucial for overall metabolic stability. Stability of the CBBC has, thus, an immediate influence on the plant's ability to cope with environmental fluctuations, e.g. changes in light intensity or temperature.

Perturbed or affected metabolic regulation can have significant effects on the rate of carbon assimilation. For example, accumulation of triose phosphates through a low starch and sucrose synthesis rate would result in low abundance of inorganic phosphate and thus limit RuBP regeneration through a lower rate of photophosphorylation (Sharkey 1985). In contrast, if triose phosphate utilization is too high, the rate at which RuBP needs to be regenerated is jeopardized as the CBBC becomes carbon-starved (Kadereit *et al.* 2014). The rate at which Rubisco fixes carbon depends on both the CO_2 and O_2 concentration at the active site of Rubisco (Warburg 1920; Foyer *et al.* 2009). This is a result of the dual catalytic function of Rubisco, which not only carboxylates RuBP, but also reacts with oxygen to form one molecule 2-PG and one of 3-PGA (Bowes *et al.* 1971; Foyer *et al.* 2009). As 2-PG is a strong inhibitor of several essential enzymes involved in the CBBC and chloroplast metabolism, its degradation is of utmost importance (Anderson 1971; Kelly and Latzko 1976; Flügel *et al.* 2017). Affected enzymes are triose-phosphate isomerase (TPI) which catalyses the interconversion between glyceraldehyde 3-phosphate (GAP) and dihydroxyacetone phosphate (DHAP) (Anderson 1971), SBPase which dephosphorylates sedoheptulose-1,7-bisphosphat (SBP) to sedoheptulose-7-phosphat (Sed7P) (Flügel *et al.* 2017) and phosphofructokinase (PFK) which catalyses steps in glycolysis (Kelly and Latzko 1976).

The multistep pathway responsible for interconversion of 2-PG is known as photorespiration and involves several subcellular compartments (Fig. 1), namely the chloroplast, peroxisome and mitochondria (Foyer *et al.* 2009). In this process, two molecules of 2-PG are converted into one molecule of CO_2 and one molecule of 3-PGA which can then be used in the CBBC and allows for the recovery of 75 % of carbon otherwise lost (Berry *et al.* 1978; Foyer *et al.* 2009). This process, however, comes at a substantial energetic cost to the cell: fixed carbon is again released and ATP and NAD(P)H are consumed (Foyer *et al.* 2009). Furthermore, ammonium (NH_4^+) is produced during photorespiration from which nitrogen has to be recaptured, adding further costs to the cell in the form of ATP and reduced ferredoxin (Foyer *et al.* 2009).

Historically, oxygenation of RuBP was interpreted as an unavoidable consequence of an oxygen-rich atmosphere, with photorespiration solely being the disposal of 2-PG (Lorimer and Andrews 1973). However, an increasing body of knowledge points to additional important physiological roles. To this extent, it has been suggested that photorespiration has a significant impact on protection from photoinhibition (Heber and Krause 1980; Takahashi *et al.* 2007; Shi *et al.* 2022). Additionally, photorespiration interacts with several other metabolic pathways and operates in a tightly regulated manner with nitrogen, sulfur and C_1 metabolism (Hodges *et al.* 2016). Yet, it still remains elusive what stabilizing or destabilizing effect photorespiration has on the CBBC. It is further questioned if 2-PG, in its function as a key regulator, can mitigate the consequences of environmental perturbations. As regulation of the CBBC is crucial for stability of whole-plant metabolism, this study aimed to investigate and quantify to what extent photorespiration affects the stability of the CBBC. For its analysis, the stability of CBBC and photorespiration was evaluated using SKM. Additionally, a discrete-parameter optimization approach was introduced being based on a modified version of the Branch and Bound (BnB) algorithm (Land and Doig 1960). To demonstrate this approach, we reevaluate the stability of the CBBC, considering regulation by 2-PG in context of other regulatory interactions.

2. MATERIALS AND METHODS

In the following section, vectors are annotated in lowercase, v. Matrices are annotated in capital letters, M.

2.1 Stability of reaction networks

Biochemical reaction networks can be deterministically described over time t by a system of ODEs, $\dot{x} = f(x, k, t)$ with $x = (x_1, ..., x_n)^T$ variables (e.g. substrate concentrations), $f = (f_1, ..., f_n)^T$ functions and $k = (k_1, ..., k_l)^T$ parameters (e.g. kinetic constants) (Klipp *et al.* 2016).

If the point x fulfils the steady-state condition $\dot{x} = 0$ ($\dot{x}_1 = 0, ..., \dot{x}_n = 0$), the system will remain in its current state without external perturbations and x is annotated as $\bar{x}$. If the system x is perturbed, the steady state can either be stable (x returns to steady state), unstable (x leaves steady state) or metastable (behaviour is indifferent) depending on the system behaviour (Klipp *et al.* 2016).

The dynamics of an ODE system $\dot{x}$ close to a stable point $\bar{x}$ can be investigated by means of linearization. To this end, the Jacobian Matrix J is obtained by Taylor expansion of temporal changes of the deviations from the steady state $\bar{x}$ and is evaluated at $\bar{x}$. The best linear approximation of $\dot{x}$ near $\bar{x}$ is then given by $\dot{x} \approx Jx + z$ with $z = (z_1, ..., z_n)^T$ containing inhomogeneities (Klipp *et al.* 2016). For non-homogenous systems (i.e. $z \neq 0$) the linearization can be converted into a homogenous

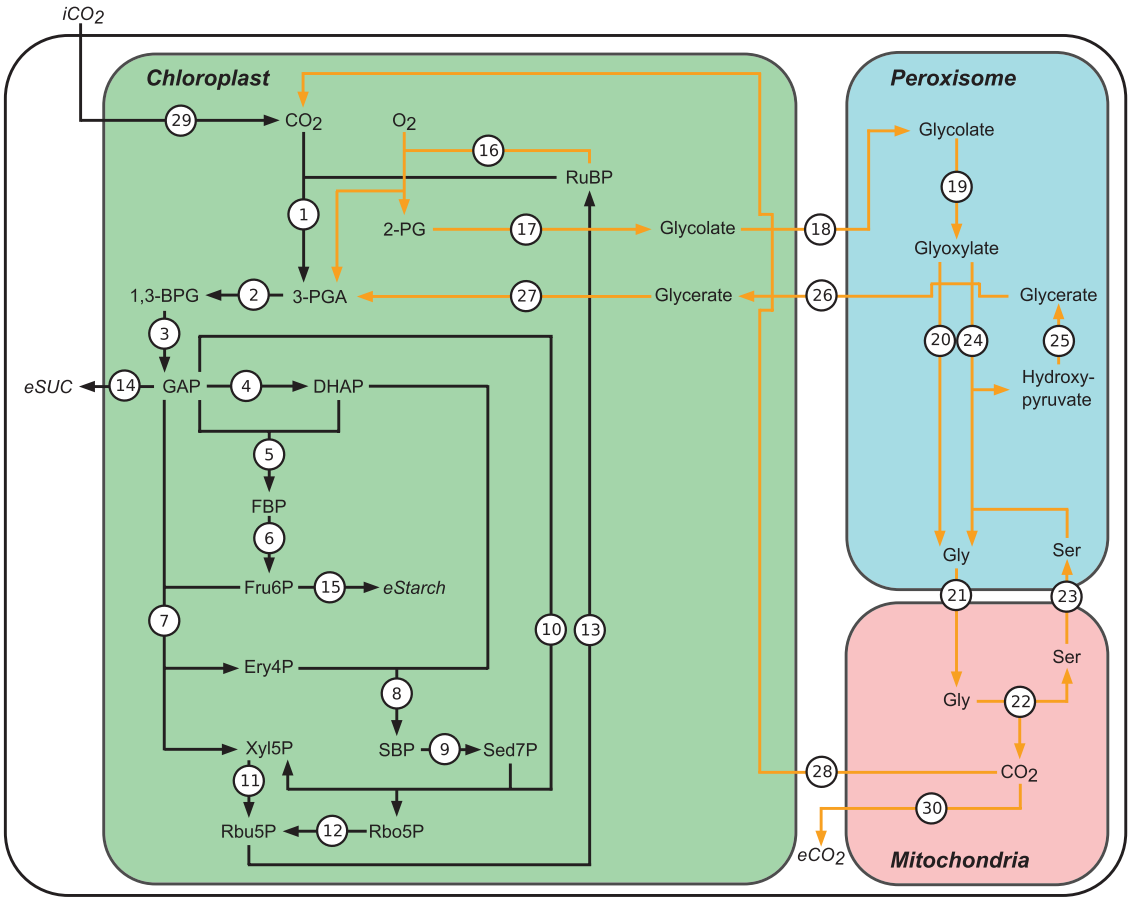

Figure 1. The Calvin–Benson–Bassham cycle (black) and photorespiration (orange). Reactions are catalysed by the following enzymes: 1. Rubisco—ribulose-1,5-bisphosphate carboxylase/oxygenase, 2. PGK—phosphoglycerate kinase, 3. GAPDH—glyceraldehyde 3-phosphate dehydrogenase, 4. TPI—triose-phosphate isomerase, 5. ALD—aldolase, 6. FBPase—fructose 1,6-bisphosphatase, 7. TK—transketolase, 8. ALD—aldolase, 9. SBPase—sedoheptulose-1,7-bisphosphatase, 10. TK—transketolase, 11. RPE—ribulose-phosphate epimerase, 12. RPI—ribose-5-phosphate isomerase, 13. PRK—phosphoribulokinase, 14. GAP export for sucrose synthesis, 15. Fru6P export for starch synthesis, 16. Rubisco—ribulose-1,5-bisphosphate carboxylase/oxygenase, 17. PGP—phosphoglycolate phosphatase, 18. Glycolate transport, 19. GO—glycolate oxidase, 20. GGAT—glutamate-glyoxylate aminotransferase, 21. Glycine transport, 22. GDC and SHMT—glycine decarboxylase complex and serine hydroxymethyltransferase, 23. Serine transport, 24. SGAT—serine-glyoxylate aminotransferase, 25. HPR1—hydroxypyruvate reductase 1, 26. Glycerate transport, 27. GLYK—glycerate kinase, 28. Portion of CO_2 reentering chloroplast, 29. CO_2 entering chloroplast from atmosphere, 30. Portion of CO_2 released to cytoplasm. RuBP—ribulose-1,5-bisphosphate, 3-PGA—3-phospho-D-glycerate, 1,3-BPG—1,3-bisphosphoglyceric acid, GAP—glyceraldehyde 3-phosphate, DHAP—dihydroxyacetone phosphate, FBP—fructose 1,6-bisphosphate, Fru6P—fructose 6-phosphate, Ery4P—erythrose 4-phosphate, Xyl5P—xylulose 5-phosphate, SBP—sedoheptulose-1,7-bisphosphate, Sed7P—sedoheptulose-7-phosphate, Rbu5P—ribulose 5-phosphate, Rbo5P—ribose-5-phosphate, 2-PG—2-phosphoglycolate, Gly—glycine, Ser—serine. The model does not consider refixation of ammonium.

system by the coordination transformation $\hat{x} = x - \bar{x}$ resulting in $(d/dt)\hat{x} = J\hat{x}$ and the general solution for homogenous systems:

$$\hat{x}(t) = \sum_{i=1}^{n} c_i b_i e^{\lambda_i t} \tag{1}$$

with λ_i being the eigenvalues of J and b_i being the corresponding eigenvectors (Klipp *et al.* 2016). The coefficients c_i can be determined by solving $x(0) = \sum_{i=1}^{n} c_i b_i$ (note that $e^{\lambda_i 0} = 1$). As a consequence of $e^{\lambda t} = e^{(a+ib)t} = e^{at}(\cos bt + i \sin bt)$, the stability of the steady state is entirely determined by the real parts of the eigenvalues of J. If all real parts of the eigenvalues are below zero (i.e. $a < 0$) then for $t \to \infty$ the term $e^{\lambda t}$ converges to 0 and thus $\hat{x}(t) \to 0$ and $x(t) \to \bar{x}$. In other words, after a perturbation the system returns to $\bar{x}$ and the steady state is considered locally asymptotically stable. If any of the eigenvalues has a positive real part (i.e. $a > 0$), the system will exponentially diverge from its steady state.

An important note is that, following the Hartman–Grobman theorem, the linearized system only reflects the local behaviour of the dynamic system if the stable point $\bar{x}$ is hyperbolic (i.e. J cannot have eigenvalues whose real parts equal 0, $a \neq 0$).

2.2 Structural kinetic modelling

In practice, calculation of the Jacobian Matrix J is often complicated by a lack of knowledge on enzymatic rate equations and kinetic parameters (e.g. V_{max}, K_m, K_i) required for the formulation of the ODE system $\dot{x}$. To circumvent this, an approach named 'SKM' was proposed by Steuer and co-workers in which kinetic

parameters are replaced by normalized enzymatic parameters (Steuer *et al.* 2006).

In this approach the system of ODEs is given by:

$$\dot{x} = \frac{dx(t)}{dt} = Nv(x,k) \tag{2}$$

with $x = (x_1, ..., x_n)^T$ metabolites and $v = (v_1, ..., v_r)^T$ reaction rates. The $n \times r$ dimensional matrix N represents the stochiometric matrix of the considered metabolic reaction network. After defining:

$$c_n(t) := \frac{x_n(t)}{\bar{x}_n}, \quad \Lambda_{nr} := N_{nr}\frac{v_r(\bar{x})}{\bar{x}_n}, and \mu_r(c) := \frac{v_r(x)}{v_r(\bar{x})}, \tag{3}$$

the variable substitution $x_n = c_n\bar{x}_n$ leads to the system being rewritten in terms of $c(t)$ as:

$$\frac{dc}{dt} = \Lambda\mu(c). \tag{4}$$

Now J can be evaluated at steady state $c^0 = 1$ with:

$$J_c = \Lambda \frac{\partial\mu(c)}{\partial c}\Big|_{c^0=1} =: \Lambda\theta_c^{\mu}. \tag{5}$$

Thus, the Jacobian is defined as a product of matrices $\mathbf{\Lambda}$ and θ. The matrix $\mathbf{\Lambda}$ consists of the stochiometric matrix N normalized to the flux $v(\bar{x})$ and metabolite concentrations $\bar{x}$ at steady state. The $r \times n$ dimensional matrix θ contains normalized elasticities and represents the degree of saturation of the normalized flux $\mu(c)$ with respect to the normalized concentration $c(t)$. Hence, entries in θ describe to what extend changes in concentration of metabolite n influence the flux rate of reaction r. Depending on the interaction between the considered metabolite and reaction, θ is either defined within the interval $(0;\ 1)$ for activating effects or within $(-1;\ 0)$ for inhibitory effects. A detailed discussion concerning entries of θ has been provided earlier (Steuer *et al.* 2006). Entries in relation to Michaelis–Menten kinetics have been discussed in Reznik and Segrè (2010).

To analyse the system dynamics, the model was repeatedly simulated with parameters for $\theta_{Substrate}^{Reaction}$ being chosen from a uniform distribution in the unit interval $(0; 1)$. This ensured that all possible explicit kinetic models of the observed system are considered. Eigenvalues of randomized Jacobians were calculated and the stability of the model was evaluated. The maximum real part of all eigenvalues represented the spectral abscissa of J.

2.3 Ranking of parameters

Parameters used in the SKM approach were ranked according to their Pearson correlation to the spectral abscissa. Additionally, the distance between the distribution function of stable solution and the original probability density function was used for ranking. Pearson correlation was calculated as follows:

$$r_{\theta b} = \frac{\sum_{i=1}^{n}(\theta_i-\bar{\theta})*(b_i-\bar{b})}{\sqrt{\sum_{i=1}^{n}(\theta_i-\bar{\theta})^2}\sqrt{\sum_{i=1}^{n}(b_i-\bar{b})^2}} \tag{6}$$

with $b = max(Re(\lambda))$. The rank for the correlation analysis R_c for a parameter $\theta_{Metabolite}^{Reaction}$ is given in descending order of $|r_{\theta b}|$. The distance was calculated by:

$$d_n = \|F_n - F_0\| = sup_x|F_n(x) - F_0(x)| \tag{7}$$

with F_n being the cumulative distribution function of values of θ resulting in a stable solution. F_0 is the cumulative normal distribution (a normal distribution was used to sample θ). Finally, sup_x is the supremum of the set of distances. The distance d_n was then ranked in descending order, yielding R_d. The overall rank for a parameter was given in ascending order of the mean from the ranks R_c and R_d.

2.4 BnB algorithm

To analyse how regulation affects the observed stability of a model, a discrete-parameter optimization algorithm was developed. It followed the *Branch and Bound* procedure first proposed by (Land and Doig 1960), which allows for the implicit enumeration of all possible combinations of regulatory interactions in a given model. In this approach, the regulatory solutions can be envisioned as forming a tree in which low performing branches are pruned. This is achieved by comparing branching nodes to a boundary value, which is determined by the heuristic solution. The algorithm uses a best-first search strategy with wide branching as reviewed before (Morrison *et al.* 2016). An added challenge arose from the fact that the objective of the optimization problem (proportion of stable solutions) was not easily calculated by a simple cost function but rather had to be determined using a Monte Carlo experiment which is inherently noisy. Owing to this, nodes were pruned by hypothesis testing. As the proportion of stable solutions follows a binomial distribution which can be normally approximated, the Z-test was used ($H_0: p_1 \leq p_2$, the proportion of stable solutions of the heuristic solution is equal or less than that of the considered node. $H_1: p_1 > p_2$, the proportion of stable solutions of the heuristic solution is greater than that of the considered node). The standard score was calculated applying the following equation (Equation 8):

$$z = \frac{\hat{p}_1 - \hat{p}_2}{\sqrt{\hat{p}(1-\hat{p})\frac{2}{n}}} \tag{8}$$

with $\hat{p}_1$ being the proportion of stable solutions within the best heuristic solution (i.e. the best solution with only discrete parameters). The proportion of stable solutions in the node considered for pruning was given by $\hat{p}_2$. The pooled standard error was calculated using $\hat{p} = (\hat{p}_1 + \hat{p}_2)/2$. The number of samples within each Monte Carlo experiment was given by n. If the value of $z > 2.33$ ($\alpha = 0.01$, one-tailed), then H_0 could be discarded (i.e. the proportion of stable solutions in the heuristic solution is significantly higher than in the observed node) and the considered node was pruned.

For continuous parameter optimization of nodes, particle swarm optimization was applied (Kennedy and Eberhart 1995). The velocity v_i and position x_i of a particle i was updated according to the particles best position p_i and the best global position p_g following:

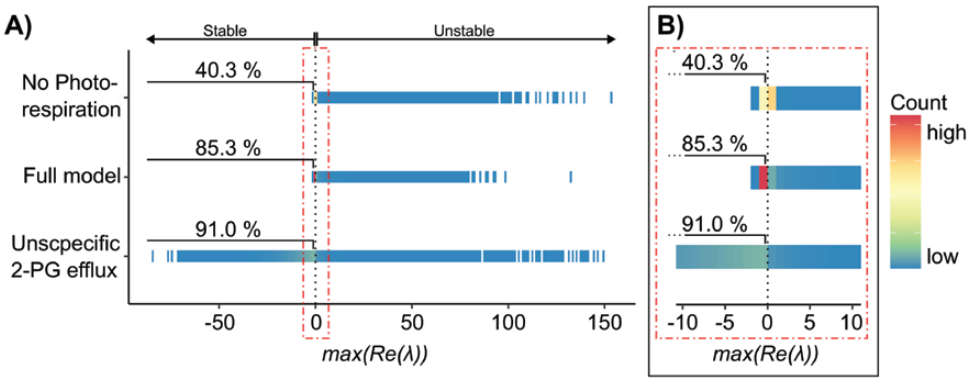

Figure 2. Stability of the CBBC. (A) Full range of spectral abscissa. (B) Enlarged view of range between −10 and 10. Results are shown for models with photorespiration, without photorespiration, and with an unspecific 2-PG efflux. Maximal real eigenvalues below 0 (dotted black line) correspond to stable systems. Each model was simulated 10^6 times. Input and saturation parameters were randomized.

$$\begin{cases} v_i \leftarrow \chi(v_i + u(0,\phi_1) \otimes (p_i - x_i) + u(0,\phi_2) \otimes (p_g - x_i)), \\ x_i \leftarrow \ x_i + v_i \end{cases} \tag{9}$$

with $\phi = \phi_1 + \phi_2 = 4.1, \quad \phi_1 = \phi_2$ and $\chi = 2/(\phi - 2 + \sqrt{\phi^2 - 4\phi})$ as proposed by (Clerc and Kennedy 2002) and reviewed in Poli *et al.* (2007). The vector $u(0,\phi)$ contained random numbers uniformly distributed in $[0,\phi]$. The numbers were randomly generated for each particle in each iteration. Component-wise multiplication is indicated by $\otimes$.

Both pseudocode of the algorithm and an accompanying MATLAB® (www.themathworks.com) script are provided in Supporting Information.

3. RESULTS

3.1 Photorespiration affects stability of carbon fixation

As plant metabolism comprises a complex network of pathways which was not possible to consider completely within this study, a simplified mathematical model was developed to simulate fluxes under the steady-state assumption, $\dot{x} = 0$. While a steady-state assumption ignores concentration dynamics in accumulating and/or depleting metabolite pools, it still reflects a helpful approximation of many pathways which show quasi-stationary concentrations without significant fluctuation, e.g., during the light or dark phase of a diurnal cycle (Gibon *et al.* 2004; Küstner *et al.* 2019b). Yet, as outlined earlier, also dynamic pathways might be interpreted based on a steady-state assumption within a (very) short time period which does not show significant alteration of metabolite concentrations (Nägele et al. 2014, 2016). The considered equilibrium point $\bar{x}$ was hyperbolic and, in accordance with the Hartman–Grobman theorem, could be used to analyse the local behaviour of the dynamical system (Hartman 1960), justifying the use of the SKM approach.

Based on real parts of eigenvalues of Jacobian matrices, the stability of the model was then analysed and compared to a model in which Rubisco only catalyses the carboxylation of RuBP (no photorespiration). In a synthetic scenario, stability was analysed under conditions where 2-PG had an unspecific efflux and no carbon was recovered. A graphical representation of these models can be found in Supporting Information—**Fig. S1**. Model simulations were run 10^6 times with metabolite concentrations and reaction fluxes being based on literature data (Flügel *et al.* 2017; Fürtauer *et al.* 2019; Jablonsky *et al.* 2011; Kitashova *et al.* 2021; Zhu *et al.* 2007; Küstner *et al.* 2019a). In conflicting reports, values from subcellular studies were used. Furthermore, input fluxes and efflux partitioning were perturbated to simulate differing physiological conditions resulting from a changing environment, e.g. stress could impose an increased ATP demand, which was reflected by perturbated efflux partitioning.

In the most basic case of all $\theta_{Substrate}^{Reaction}$ being set to 1 (corresponding to simple irreversible mass-action kinetics), the full model (including all reactions shown in Fig. 1) and the model with an unspecific 2-PG efflux showed a stable steady state. In contrast, the model without photorespiration demonstrated an unstable steady state (Fig. 2).

When allowing $\theta_{Substrate}^{Reaction}$ to move freely in the interval (0; 1), the results indicated that the model without photorespiration was the least stable with only 40.3 % of simulations resulting in a stable solution, i.e. $max(Re(\lambda))$ was negative (Fig. 2). Comparison to the full model showed that including the photorespiratory pathway stabilized the system to 85.3 %. Interestingly, the most stable model was observed with an unspecific efflux of 2-PG where 91.0 % of the spectral abscissa (the maximum real part of all eigenvalues) were below 0. Additionally, this model possessed large negative eigenvalues and thus converged faster than the two other models. It is, however, important to keep in mind that such a scenario is highly artificial and would significantly reduce carbon assimilation rates. Due to the proportion of stable solutions (91 % vs. 40.3 %), these results suggested that oxygenation of RuBP increases stability of the CBBC. Furthermore, the convergence rate was increased resulting in a faster response to perturbations. As this stabilizing effect was seen in both the full model and the model with an unspecific efflux, this suggested that the observed stabilization did not result from the addition of an arbitrary cyclic structure but rather from the oxygenation of RuBP. The multistep process of recuperating carbon from 2-PG again resulted in a slow convergence rate, yet the higher proportion of stable solutions was maintained. Photorespiration

Table I. Ranking of saturation coefficients θ in accordance with their impact on the stability. Rankings are provided both with respect to the full model and the model lacking photorespiration. Rank 1: highest impact, rank 34: lowest impact. θ represents the saturation coefficient between a given metabolite and a reaction. Pearson correlation and the distance measure dn between the cumulative distribution function of values of θ resulting in a stable solution and the original distribution function were used for ranking.

	Full model			No Photorespiration		
Overall rank	**θ**	***Correlation***	**dn**	**θ**	***Correlation***	**dn**
1	θGAPTPI	-0.28	0.0637	θGAPTPI	-0.07	0.2454
2	θGAPTK	0.15	0.0366	θGAPeSuc	-0.05	0.2892
3	θFru6PTK	-0.12	0.0268	θCO2Rubisco	-0.11	0.0102
4	θGAPeSuc	-0.12	0.0339	θGAPTK	0.04	0.1016
5	θ3PGAPGK	0.08	0.0092	θRuBPRubisco	0.04	0.0028
6	θRuBPRubisco	0.06	0.0058	θFru6PTK	-0.01	0.0121
7	θGAPTK	0.04	0.0074	θ3PGAPGK	0.02	0.0021
8	θGlyoxylateSGAT	0.03	0.0187	θGAPAld	-0.01	0.0026
9	θGlyoxylateGGAT	-0.02	0.0350	θGAPTK	0.02	0.0017
10	θSed7PTK	-0.03	0.0073	θSed7PTK	-0.01	0.0027
11	θDHAPALD	0.04	0.0032	θEry4PALD	0.01	0.0017
12	θSBPSBPase	0.02	0.0037	θFru6PeStarch	0.00	0.0032
13	θSerMitSerT	-0.02	0.0041	θDHAPALD	0.01	0.0014
14	θSerPerSGAT	-0.01	0.0094	θDHAPAld	0.00	0.0024
15	θCO2Rubisco	-0.03	0.0026	θRbo5PRPI	0.01	0.0015
16	θEry4PALD	0.02	0.0028	θ13BPGPGK	0.00	0.0015
17	θGAPAld	-0.03	0.0018	θRbu5PPRK	0.00	0.0017
18	θDHAPAld	-0.01	0.0024	θSBPSBPase	0.01	0.0012
19	θGlycerateChlGLYK	0.01	0.0046	θXyl5PRPE	0.01	0.0012
20	θGlycolateChlGlycoT	0.01	0.0029	θFBPFBPase	0.00	0.0014
21	θHydroxyp.HPR	0.01	0.0035			
22	θCO2_miteCO2	-0.01	0.0044			
23	θRbo5PRPI	0.01	0.0020			
24	θGlyceratePerGlycertaeT	0.01	0.0035			
25	θGlycolatePerGO	0.01	0.0020			
26	θCO2_mitCO2_d	0.01	0.0031			
27	θGlyPerGlyT	0.01	0.0019			
28	θXyl5PRPE	0.01	0.0011			
29	θRbu5PPRK	0.01	0.0010			
30	θGlyMitGDC/SHMT	0.01	0.0011			
31	θ13BPGPGK	0.00	0.0016			
32	θFru6PeStarch	0.00	0.0018			
33	θ2PGPGP	0.00	0.0016			
34	θFBPFBPase	0.00	0.0010			

thus increased the probability of finding a stable steady state at experimentally observed metabolite concentrations and reaction fluxes.

3.2 GAP dynamics are pivotal for system stability

One of the draw backs of the SKM approach lies in the fact that *in vivo* only a subset of the analysed parameter space is present. Owing to this and in order to investigate where the 14.7 % instability observed in the full model originated from, perturbed parameters of the model were ranked in accordance to their impact on the stability of the metabolic network. This allowed us to estimate the physiological relevance of the results. Pearson correlation between parameters and $max(Re(\lambda))$ was determined. Furthermore, the distribution of perturbed parameter values resulting in a stable solution was compared to their original probability density function, $\|d_n = F_n - F_0\|$. In the full model, the most influential parameters were almost all found to be tied to reactions and metabolites within the CBBC (Table 1). An exception to this were parameters which determine the effect of glycolate on rates of GGAT and SGAT ($\theta^{GGAT}_{Glyoxylate}$, $\theta^{SGAT}_{Glyoxylate}$). These parameters were associated with photorespiration rather than the CBBC. However, the results showed that reactions involving GAP as a substrate (θ^{TPI}_{GAP}, θ^{TK}_{GAP}, θ^{eSuc}_{GAP}) were the most essential in stabilizing the system after perturbation. This observation was true for both the full model as well as the model ignoring photorespiration. To a lesser extent, this was

also observed for the carboxylation and oxygenation of RuBP ($\theta^{Rubisco}_{RuBP}$, $\theta^{Rubisco}_{CO2}$). However, this was more pronounced in the model lacking photorespiration. In conclusion, this suggested that GAP partitioning was the most essential aspect governing CBBC stability.

Interestingly, reactions catalysed by TPI, and to a lesser extend also SBPase, had a considerable impact on the stability of the model. This further suggested a possible benefit of inhibition by 2-PG which inhibits both enzymes.

Comparing parameters between both models revealed a sharp increase in the value of d_n for two parameters, θ^{TPI}_{GAP} and θ^{eSuc}_{GAP}. The d_n value for θ^{eSuc}_{GAP} increased from 0.037 to 0.289, for θ^{TPI}_{GAP} the change was slightly lower, increasing from 0.064 to 0.245. This increase was coupled with a decline in the corresponding correlation coefficients. As d_n represents a shift in the parameter distribution found in stable solutions from the uniform distribution, this was most likely the consequence of a reduced parameter space leading to stable solutions. Values of θ contained in stable solutions were compared between the two models (Fig. 3).

The lack of photorespiration clearly reduced the parameter space of stable solutions compared to the full model. Values of the saturation parameter θ^{eSuc}_{GAP} were shifted towards 1, while θ^{TPI}_{GAP} was shifted towards 0. This suggested an increasing importance of GAP export in order to stabilize the system, especially in relation to GAP utilization for DHAP synthesis. As starch synthesis occurs downstream of TPI, this indicated that starch synthesis may not be able to stabilize fluctuations effectively. Taken together, the structure and location of photorespiration thus appeared to alleviate the pressure on the GAP export required to stabilize the system.

Previous studies and the rich history of explicit modelling of the CBBC and photorespiration showed that TPI operates close to equilibrium under physiological conditions (Jablonsky *et al.* 2011). This suggested that θ^{TPI}_{GAP} should be closer to 1 (as was found in the full model) which indicated that the reduced proportion of stable solutions (see Fig. 2) was indeed of importance in relation to conditions *in vivo*. However, it is important to consider that this would also be reflected in a value of θ^{TPI}_{DHAP} close to −1, suggesting reversibility. To ensure that reduced parameter space of θ^{TPI}_{GAP} was still relevant under these reversible conditions, the two models were simulated reflecting this change and distributions of θ^{TPI}_{GAP} and θ^{eSuc}_{GAP} were again compared [**see Supporting Information—Fig. S2**]. Previous observations were confirmed with this approach suggesting that the observed stabilizing effect of photorespiration was not an artefact of an irreversibility assumption but indeed relevant under physiological conditions.

Following this, the model was investigated to analyse if starch synthesis was indeed unable to affect the stability of the system. The effect of $\theta^{eStarch}_{Fru6P}$ on the stability was analysed across the two models (Table 1). Both models showed no apparent effect of $\theta^{eStarch}_{Fru6P}$ for the stability of the system. A change in θ^{eSuc}_{GAP} had a direct effect on the partial derivative $\frac{\partial(f(GAP))}{\partial(GAP)}$ found within the Jacobian matrix. As a result of Equation (5), higher values of θ^{eSuc}_{GAP} resulted in an absolute increase of $\frac{\partial(f(GAP))}{\partial(GAP)}$, thus increasing the effect that a change in the concentration of GAP had upon its own dynamics. Furthermore, θ^{eSuc}_{GAP} only affected $\frac{\partial(f(GAP))}{\partial(GAP)}$, whereas changes in other parameters of GAP also affected other entries in the Jacobian (e.g. θ^{TPI}_{GAP} affects $\frac{\partial(f(GAP))}{\partial(GAP)}$ and $\frac{\partial(f(DHAP))}{\partial(GAP)}$). This could make GAP dynamics more resilient against effects of other metabolites and might constitute an overflow mechanism for excess carbon out of the CBBC without influencing CBBC dynamics. Similarly, an increase in $\theta^{eStarch}_{Fru6P}$ affected $\frac{\partial(f(Fru6P))}{\partial(Fru6P)}$, allowing more control over its own dynamics. However, as mentioned previously, the most crucial junction determining the stability was found to be at GAP and its various pathways. Thus, an increase in the absolute value of $\frac{\partial(f(GAP))}{\partial(GAP)}$ appeared to be more beneficial than an absolute increase in $\frac{\partial(f(Fru6P))}{\partial(Fru6P)}$.

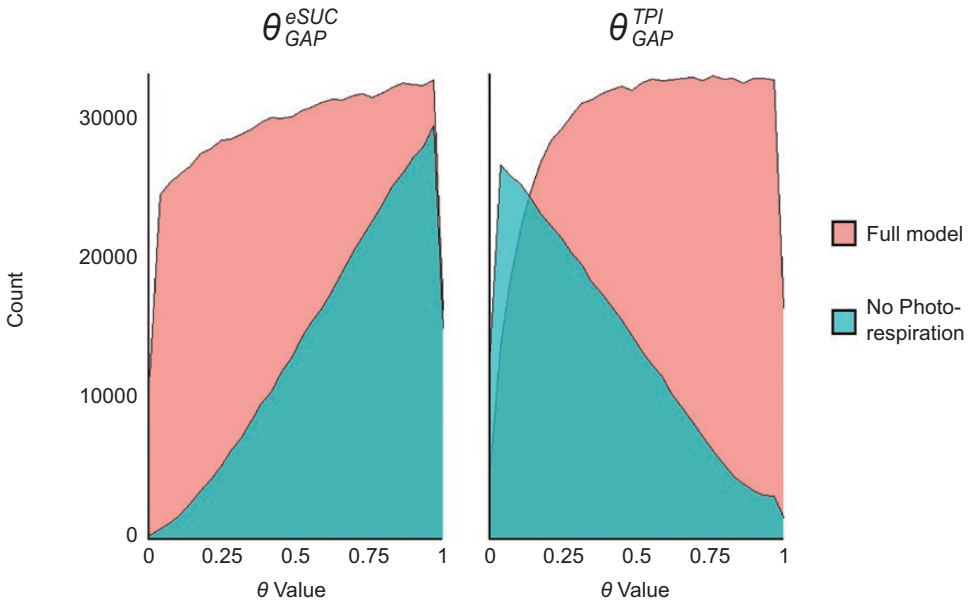

Figure 3. Values of θ found in stable solutions. Parameters are shown in which the model without photorespiration showed the largest deviation from the expected distribution ($d_n\theta^{eSuc}_{GAP} = 0.289$, $d_n\theta^{TPI}_{GAP} = 0.245$). Values for θ are shown for both the full model and the model excluding photorespiration.

3.3 A shift in carbon partitioning towards sucrose synthesis increases metabolic stability

Based on the assumption that an increase in the absolute value of $\frac{\partial(f(GAP))}{\partial(GAP)}$ may stabilize the CBBC, it was suggested that an increase in the ratio of assimilated carbon going to sucrose biosynthesis rather than starch synthesis should increase the stability of the model as well. This would be a consequence of Equation (10).

$$\frac{\partial(f(GAP))}{\partial(GAP)} = \sum_{j=1}^{m} \Lambda_j^{GAP} * \theta_{GAP}^{j}, \tag{10}$$

The resulted from rules of matrix multiplication when analysing a single element of J following Equation (5). Following the term $\Lambda_{eSuc}^{GAP} * \theta_{GAP}^{eSuc} = -1 * \frac{v_{eSuc}[GAP]}{[GAP]} * \theta_{GAP}^{eSuc}$, a shift of assimilated carbon towards sucrose synthesis rather than starch synthesis increased $v_{eSuc}[GAP]$ and, thus, $\frac{\partial(f(GAP))}{\partial(GAP)}$, resulting in a similar effect as observed above. To test this, the ratio of sucrose/starch allocation was shifted in the model by altering the corresponding fluxes and the results were again simulated 10^6 times for each condition.

Supporting the hypothesis, results showed that an increased proportion of sucrose biosynthesis resulted in an increase in the stability of the system (Fig. 4). Interestingly, this effect was more pronounced under deficiency of photorespiration (24.4 % → 46.2 % stability vs. 79.8 % → 86.1 % stability, see Fig. 4).

In addition to increased biosynthesis of soluble sugars, accumulation of secondary metabolites is a well-known stress and acclimation response of plants (see e.g. Winkel-Shirley 2002; Doerfler *et al.* 2013). Following the finding that a shift from starch towards sucrose synthesis was able to stabilize the system, a model was created containing an Ery4P export to simulate the impact that induction of secondary metabolism via the shikimate pathway might have on the CBBC. A graphical representation of this model and a model containing Ery4P export, but no photorespiration, is provided in **Supporting Information—Fig. S3**. Similar as to what was observed for starch metabolism, the value of $\theta_{Ery4P}^{eSecondary\_Metabolism}$ had no significant effect on the stability of the system (Table 2).

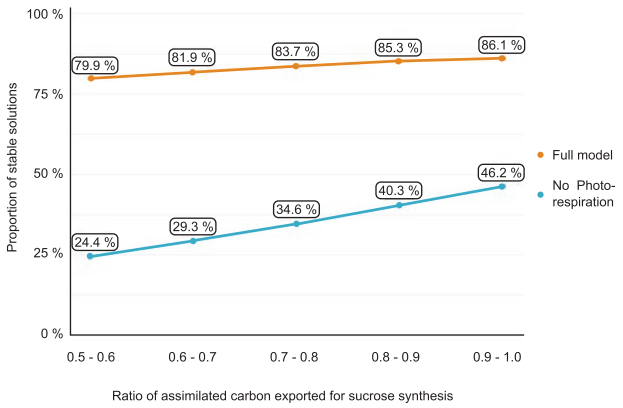

Figure 4. Portion of stable solutions with increasing carbon partitioning going towards sucrose synthesis. Each point was simulated 10^6 times at different ratios of sucrose synthesis randomized within an interval of 0.1; the ratio is given in C6-Sucrose/C6-Starch.

Table 2. Effect of $\theta_{Ery4P}^{eSecondary\_Metabolism}$ on the stability of the CBBC. The rank of $\theta_{Ery4P}^{eSecondary\_Metabolism}$ is shown in relation to all other θ parameters involved in the model. The parameter θ in general represents the saturation coefficient between a given metabolite and a reaction. Ranking was achieved according to its Pearson correlation with the spectral abscissa and the distance measure d_n.

Model	Rank	Pearson correlation	*dn*
Full model	34 of 35	–0.01	0.001
No photorespiration	15 of 21	0.00	0.011

Based on this finding, we hypothesized that GAP export for sucrose synthesis was particularly able to stabilize the system which might result from its direct ability to control GAP dynamics. To test this hypothesis, the ratio of carbon going towards sucrose, starch or secondary metabolites was altered and the proportion of stable solutions under each condition was quantified (Fig. 5).

In presence of the photorespiratory pathway, carbon allocation towards sucrose proved to be the most effective in stabilizing the system (Fig. 5, left panel, full model). In contrast, a lack of photorespiration shifted most stable parameter combinations towards higher activity of secondary metabolism (40–60 %). In both models, carbon channelling into starch biosynthesis contributed least to stability (0–20 %). In summary, these results suggested that the presence of the photorespiratory pathway allows for higher rates of sucrose biosynthesis without compromising the stability of the metabolic network, i.e. a higher carbon flux has to be allocated towards secondary metabolism in the absence of photorespiration in order to increase metabolic stability. Further, the stabilizing effect of GAP export was only found to be efficient if a sufficiently large parameter space for GAP export was present, which might be achieved either through photorespiration or secondary metabolism [**see Supporting Information—Fig. S4**].

3.4 The role of 2-PG in stabilizing the CBBC

To analyse if regulation of the CBBC by 2-PG though inhibition of TPI and/or SBPase may change the carbon partitioning towards a more stable system, a BnB algorithm was applied with the purpose of searching for optimal strategy resulting in stable solutions. This analysis was challenged by the combinatorial problem of testing ~4 * 10^{12} parameter combinations. Here, BnB enabled a computation time of, in total, <700 h (MATLAB® R2021a, Intel® Core™ i7-10700 @ 2.90 GHz).

In a situation where no enzymatic regulation, except for TPI and SBPase, was considered, both inhibition of TPI and SBPase by 2-PG lead to a decrease in stability (Fig. 6A). This effect was strongest for TPI, where the proportion of stable models fell from 85.3 % without inhibition to 6.1 % with strong inhibition. Although less pronounced, a drop of stability from 85.3 % to 80.6 % was also observed for SBPase. This drastically changed when considering full enzymatic regulation of the CBBC, highlighting the importance of the BnB approach (Fig. 6B). In 30 % of near-optimal solutions (no significant difference to the best solution, $P > 0.01$), a weak inhibition of TPI by 2-PG was observed. A weak inhibition by 2-PG of SBPase was observed in 15 % of

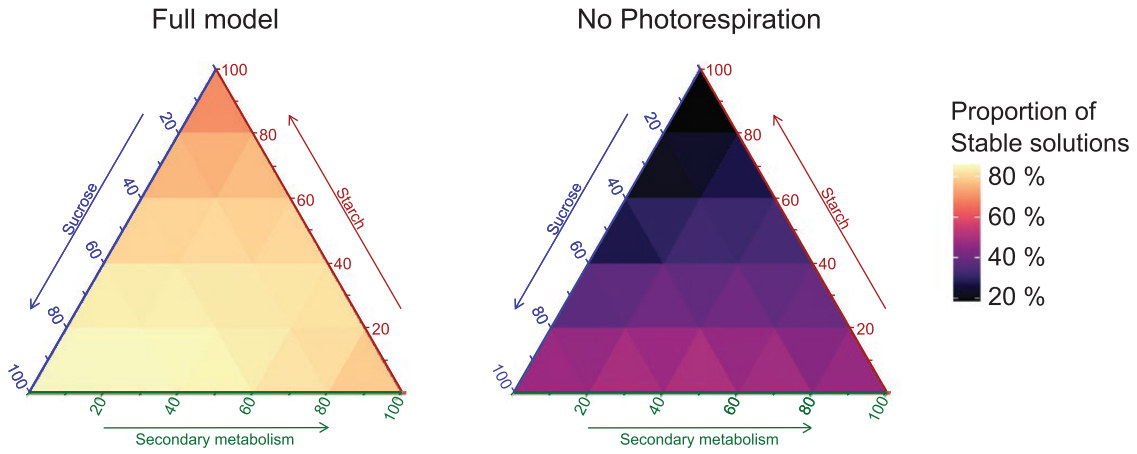

Figure 5. How carbon allocation affects the stability of the CBBC. The ternary plot was constructed from 231 data points each simulated 10^4 times per model. Arrows indicate the proportion of carbon flux in direction of sucrose, starch and/or secondary metabolites. Colour indicates proportion of stable solutions.

all simulated models and strong inhibition in 75 % of solutions. This indicated a positive effect of regulation by 2-PG on the stability of the metabolic network with inhibition of SBPase taking a key role. Although this was more ambiguous for the regulation of TPI, a considerable parameter space existed also for this inhibition (30 % of all scenarios).

4. DISCUSSION

Exposure to a sudden change of environmental conditions, e.g. light intensity or temperature, typically induces stress reactions in organisms to counteract and prevent irreversible damage of cells, tissues or organs. Stabilization of metabolism plays a central role in such stress response because it is preliminary to perceive and integrate environmental signals (Zhang *et al.* 2022). Here, stability might be interpreted as the probability of transition of metabolic steady states, and it has been shown before that stability properties can be determined by network structures themselves, e.g., by metabolic cycles (Reznik and Segrè 2010). Stability properties of a biochemical reaction network can be quantified via an SKM approach (Steuer *et al.* 2006). With this approach, effects of single and/or multiple effectors and regulators on system stability can be estimated to yield non-intuitive information about metabolic pathways, pathway structures (Reznik and Segrè 2010) or metabolic acclimation strategies (Fürtauer and Nägele 2016). In case of an unstable metabolic state, slight modifications of environmental conditions might immediately result in an oscillating, or chaotic, dynamic behaviour of single metabolite concentrations or whole pathways (Fürtauer and Nägele 2016). In photosynthetic metabolism, this might rapidly lead to an imbalance of, e.g., ATP/ADP or NADPH/NADP ratios which can easily cause generation of reactive oxygen species and tissue damage (Noctor and Foyer 2000). To reliably estimate stability properties in metabolic systems, a vast variety of regulatory interactions between proteins and metabolites needs to be considered which rapidly results in extensive combinatorial problems for computation. To overcome some limitations of computation time, we applied a discrete-parameter optimization approach. The importance of such an approach became evident when evaluating the effect of inhibition of CBBC enzymes by 2-PG which finally suggested that photorespiration represents a trade-off between carbon assimilation rate and stability of cellular metabolism. This finding is in line with previous work which came to a similar conclusion using simplified ODE models with mass-action kinetics (Hahn 1991). Furthermore, previously published work in bioengineering found that a bypass, oxidizing glycolate completely in the chloroplast, leads to a 40 % increase in biomass production of tobacco plants in field experiments (South *et al.* 2019). This further suggests that the stabilizing effect resulting from photorespiration is tied to oxygenation of RuBP rather than its innate cyclic structure. This is owing to the fact that, considering fluctuations apparent to field experiments, synthetic plants showed an increase in biomass production as compared to wild-type tobacco.

Our findings supplement and extend the previously suggested regulatory role of 2-PG for adjustment and allocation of chloroplast carbon flow (Flügel *et al.* 2017). The amount of 2-PG is tightly regulated by 2-PG phosphatase, PGLP, and its activity was shown to be essential for efficient carbon fixation and allocation (Flügel *et al.* 2017; Levey *et al.* 2019). Altogether, this suggests a strong impact of PGLP activity on stabilizing whole-cell carbon metabolism after environmental perturbation. Further, simulations revealed that differential allocation of fixed carbon in either soluble carbohydrates, storage compounds or other (secondary) metabolism differentially affects stability of the whole CBBC network. As a consequence, under sudden temperature and/or light changes, when ratios of Rubisco-driven carboxylation and oxygenation significantly deviate from the current homeostasis, metabolism needs to be reprogrammed to maximize stabilization capacities.

The capability of re-stabilizing carbon fixation, and all downstream carbohydrate biosynthesis, is a critical variable in plant ecology and evolution because it significantly determines cell and tissue fate as well as growth and developmental success. Hence, combining biochemical and physiological experiments with stability analysis, e.g. by SKM, represents a promising approach to yield detailed insights into metabolic regulation. This information is essential to interpret experimental data on metabolite dynamics because underlying regulation might comprise non-intuitive patterns, e.g. metabolic

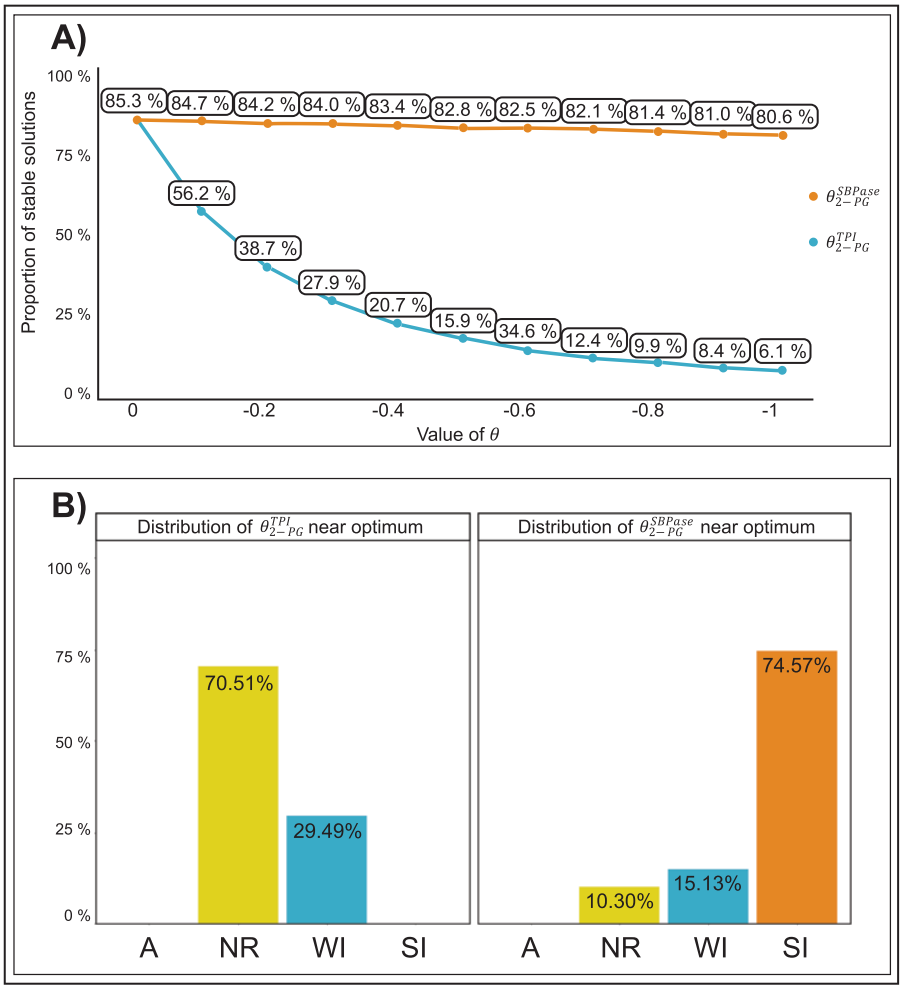

Figure 6. Effects of inhibition of TPI and SBPase by 2-PG. (A) Effects of inhibition by 2-PG without considering regulation of the CBC. Each point was simulated 10^5 times. The blue line represents the effect of 2-PG on TPI. The orange line depicts the effect of 2-PG on SBPase. (B) Effects of inhibition by 2-PG when considering regulation of the CBC. Depicted are results of parameter optimization. The bar plot shows the distribution of regulatory interactions between 2-PG and TPI or SBPase found at the optimal solution and solutions which are not significantly worse ($P > 0.01$). A: activation ($\theta = 1$), NR: no regulation ($\theta = 0$), WI: weak inhibition ($\theta = -0.1$), SI: strong inhibition ($\theta = -0.99$).

cycles (Reznik and Segrè 2010) or nested structures (Schaber *et al.* 2009) which limit interpretation of experimental findings. Further, it indicates the dependency of structural kinetic properties within a metabolic network which interconnects pathways across diverse subcellular compartments. We found that stabilization is achieved by increasing the parameter space of θ_{GAP}^{eSuc} and θ_{GAP}^{TPI} resulting in a stable solution (see Fig. 3). Owing to this and the noticeable correlation of θ_{GAP}^{eSuc} with $max(Re(\lambda))$ but not for $\theta_{Fru6P}^{eStarch}$, a shift from starch accumulation towards sucrose synthesis was able to stabilize the kinetic models (see Table 1 and Fig. 4).

It has been described earlier that under stress, e.g. due to low temperature, carbon allocation is redirected from starch to sucrose biosynthesis (Strand et al. 1997, 1999). While this can be explained by the metabolic role of soluble carbohydrates as substrates for other pathways or osmotically active substances (Obata and Fernie 2012), we hereby provide evidence for an additional role of this metabolic reprogramming in structural kinetic stabilization of carbon metabolism against environmentally induced perturbations. Owing to limitations set by this approach, only a small subset of pathways found within a cell could be analysed. For example, in the simulated models photorespiration was treated as a closed loop. The addition of further pathways (e.g. nitrogen, sulfate and C_1 metabolism), which are tightly linked to photorespiration, might lead to further regulatory insights (Hodges *et al.* 2016). The speed of convergence towards the steady state could be increased, as reflected by large negative eigenvalues, when photorespiration was treated as an open loop, which would further emphasize the stabilizing effect observed, bringing the model more towards the unrealistic scenario where 2-PG possesses an unspecific efflux (see Fig. 2).

Besides soluble carbohydrates, also secondary metabolites, e.g. flavonoids via the shikimate pathway, are well-known to be involved in plant abiotic stress reactions, acclimation and tolerance mechanisms (Winkel-Shirley 2002; Schulz *et al.* 2016; Naikoo *et al.* 2019). Yet, previously, evidence has also been provided for significant variation of the extent of accumulation of secondary metabolites even across different natural accessions of *Arabidopsis thaliana* (Schulz *et al.* 2015). While significant correlation between tolerance measures, e.g. freezing tolerance, and flavonoid metabolism has been observed in

these studies, some of the underlying mechanisms remain elusive. For example, transcript levels were found to be associated much stronger to freezing tolerance than absolute metabolite levels (Schulz *et al.* 2015). In context of findings of the present study this might highlight and support the hypothesis of metabolic stabilization by modification of efflux/influx capacities of the CBBC and photorespiratory pathways towards starch, sucrose and secondary metabolism (see Fig. 5). While our analysis revealed that in the full model partitioning of carbon towards sucrose biosynthesis improved the stability more than allocating carbon towards secondary metabolism, secondary metabolism was structurally able to provide a similar effect by increasing the admissive parameter space when oxygenation of RuBP was decreased. Finally, the optimal carbon partitioning was shifted under these conditions towards 40–50 % into secondary metabolism and 50–60 % into sucrose synthesis. Such a scenario might reflect a stress-acclimated state of plant metabolism when rates of photorespiration are decreased again after initial stress response while sugars and secondary metabolites are significantly increased in their amount (Savitch *et al.* 2001; Doerfler *et al.* 2013). It further emphasizes the regulatory interaction between pathways with differential subcellular localization and indicates how stability may affect evolution of metabolism.

In conclusion, our study suggests a stabilizing role of photorespiration on the dynamics of cellular metabolism, thus representing a trade-off between carbon assimilation and metabolic stability in a dynamic environment. Finally, shifting carbon partitioning from starch accumulation towards sucrose synthesis significantly increases system stability which might be related to stress tolerance mechanisms of plants.

SUPPORTING INFORMATION

The following additional information is available in the online version of this article—

Figure S1. Graphical representation of models. (A) Full model. (B) Model lacking photorespiration. (C) Model with unspecific 2-PG efflux.

Figure S2. Values of θ found in stable solutions for TPI reversibility. Values for θ are shown for both the full model and the model excluding photorespiration.

Figure S3. Graphical representation of models with export for secondary metabolism. (A) Full model with Ery4P export. (B) Model lacking photorespiration with Ery4P export.

Figure S4. Effect of carbon partitioning between sucrose synthesis and secondary metabolism. Top: Changes to model stability. Bottom: Effect on admissible parameter space.

MATLAB Scripts. All scripts used in this work. Each model and the Branch and Bound algorithm are present in a separate folder.

Pseudocode BnB. A brief overview of the functions involved in the Branch and Bound algorithm.

SOURCES OF FUNDING

This work was funded by Deutsche Forschungsgemeinschaft, DFG (NA 1545/4-1).

CONFLICT OF INTEREST

None declared.

CONTRIBUTIONS BY THE AUTHORS

Both authors conceptualized the study, performed modelling and calculations, and wrote the paper.

ACKNOWLEDGEMENTS

We would like to thank all members of Plant Evolutionary Cell Biology at the Faculty of Biology, LMU Munich, for many fruitful discussions. Further, we thank the Graduate School Life Science Munich for support.

LITERATURE CITED

Anderson LE. 1971. Chloroplast and cytoplasmic enzymes II. Pea leaf triose phosphate isomerases. *Biochimica et Biophysica Acta (BBA) - Enzymology* 235:237–244.

Andersson I. 2008. Catalysis and regulation in Rubisco. *Journal of Experimental Botany* 59:1555–1568.

Bassham JA, Benson AA, Kay LD, Harris AZ, Wilson AT, Calvin M. 1954. The path of carbon in photosynthesis. XXI. The cyclic regeneration of carbon dioxide acceptor1. *Journal of the American Chemical Society* 76:1760–1770.

Berry JA, Osmond CB, Lorimer GH. 1978. Fixation of $18O_2$ during photorespiration: kinetic and steady-state studies of the photorespiratory carbon oxidation cycle with intact leaves and isolated chloroplasts of C_3 plants 1. *Plant Physiology* 62:954–967.

Bisswanger H. 2017. *pH and temperature dependence of enzymes*. Berlin, Germany: Wiley–VCH Verlag, 145–147.

Bowes G, Ogren WL, Hageman RH. 1971. Phosphoglycolate production catalyzed by ribulose diphosphate carboxylase. *Biochemical and Biophysical Research Communications* 45:716–722.

Clerc M, Kennedy J. 2002. The particle swarm—explosion, stability, and convergence in a multidimensional complex space. *IEEE Transactions on Evolutionary Computation* 6:58–73.

Doerfler H, Lyon D, Nägele T, Sun XL, Fragner L, Hadacek F, Egelhofer V, Weckwerth W. 2013. Granger causality in integrated GC-MS and LC-MS metabolomics data reveals the interface of primary and secondary metabolism. *Metabolomics* 9:564–574.

Flügel F, Timm S, Arrivault S, Florian A, Stitt M, Fernie AR, Bauwe H. 2017. The photorespiratory metabolite 2-phosphoglycolate regulates photosynthesis and starch accumulation in *Arabidopsis*. *The Plant Cell* 29:2537–2551.

Foyer CH, Bloom AJ, Queval G, Noctor G. 2009. Photorespiratory metabolism: genes, mutants, energetics, and redox signaling. *Annual Review of Plant Biology* 60:455–484.

Fürtauer L, Küstner L, Weckwerth W, Heyer AG, Nägele T. 2019. Resolving subcellular plant metabolism. *The Plant Journal* 100:438–455.

Fürtauer L, Nägele T. 2016. Approximating the stabilization of cellular metabolism by compartmentalization. *Theory in Biosciences* 135:73–87.

Gibon Y, Blasing OE, Palacios-Rojas N, Pankovic D, Hendriks JH, Fisahn J, Hohne M, Gunther M, Stitt M. 2004. Adjustment of diurnal starch turnover to short days: depletion of sugar during the night leads to a temporary inhibition of carbohydrate utilization, accumulation of sugars and post-translational activation of ADP-glucose pyrophosphorylase in the following light period. *The Plant Journal* 39:847–862.

Grimbs S, Selbig J, Bulik S, Holzhütter H-G, Steuer R. 2007. The stability and robustness of metabolic states: identifying stabilizing sites in metabolic networks. *Molecular Systems Biology* 3:146.

Hahn BD. 1991. Photosynthesis and photorespiration: modelling the essentials. *Journal of Theoretical Biology* 151:123–139.

Hartman P. 1960. A lemma in the theory of structural stability of differential equations. *Proceedings of the American Mathematical Society* 11:610–620.

Heber U, Krause GH. 1980. What is the physiological role of photorespiration? *Trends in Biochemical Sciences* 5:32–34.

Hodges M, Dellero Y, Keech O, Betti M, Raghavendra AS, Sage R, Zhu X-G, Allen DK, Weber APM. 2016. Perspectives for a better understanding of the metabolic integration of photorespiration within a complex plant primary metabolism network. *Journal of Experimental Botany* 67:3015–3026.

Jablonsky J, Bauwe H, Wolkenhauer O. 2011. Modeling the Calvin–Benson cycle. *BMC Systems Biology* 5:185.

Kadereit JW, Körner C, Kost B, Sonnewald U. 2014. *Strasburger – lehrbuch der pflanzenwissenschaften*. Heidelberg: Springer Spektrum Berlin.

Kelly GJ, Latzko E. 1976. Inhibition of spinach-leaf phosphofructokinase by 2-phosphoglycollate. *FEBS Letters* 68:55–58.

Kennedy J, Eberhart R. 1995. Particle swarm optimization. Proceedings of ICNN'95-International Conference on Neural Networks, Perth, WA, Australia. 4:1942–1948. doi:10.1109/ICNN.1995.488968.

Kitashova A, Schneider K, Fürtauer L, Schröder L, Scheibenbogen T, Fürtauer S, Nägele T. 2021. Impaired chloroplast positioning affects photosynthetic capacity and regulation of the central carbohydrate metabolism during cold acclimation. *Photosynthesis Research* 147:49–60.

Klipp E, Liebermeister W, Wierling C, Kowald A. 2016. *Systems biology: a textbook*. Weinheim: Wiley-VCH.

Küstner L, Fürtauer L, Weckwerth W, Nägele T, Heyer AG. 2019a. Subcellular dynamics of proteins and metabolites under abiotic stress reveal deferred response of the *Arabidopsis thaliana* hexokinase-1 mutant gin2-1 to high light. *The Plant Journal* 100:456–472.

Küstner L, Nägele T, Heyer AG. 2019b. Mathematical modeling of diurnal patterns of carbon allocation to shoot and root in *Arabidopsis thaliana*. *npj Systems Biology and Applications* 5:4.

Land A, Doig A. 1960. An automatic method of solving discrete programming problems. *Econometrica* 28:497–520.

Levey M, Timm S, Mettler-Altmann T, Luca Borghi G, Koczor M, Arrivault S, Pm Weber A, Bauwe H, Gowik U, Westhoff P. 2019. Efficient 2-phosphoglycolate degradation is required to maintain carbon assimilation and allocation in the C_4 plant *Flaveria bidentis*. *Journal of Experimental Botany* 70:575–587.

Lorimer GH, Andrews TJ. 1973. Plant photorespiration—an inevitable consequence of the existence of atmospheric oxygen. *Nature* 243:359–360.

Martin W, Scheibe R, Schnarrenberger C. 2000. The Calvin cycle and its regulation. In: Leegood RC, Sharkey TD, von Caemmerer S, eds. *Photosynthesis: physiology and metabolism*. Dordrecht: Kluwer Academic Publishers, 9–51.

Morrison DR, Jacobson SH, Sauppe JJ, Sewell EC. 2016. Branch-and-bound algorithms: a survey of recent advances in searching, branching, and pruning. *Discrete Optimization* 19:79–102.

Nägele T, Fürtauer L, Nagler M, Weiszmann J, Weckwerth W. 2016. A strategy for functional interpretation of metabolomic time series data in context of metabolic network information. *Frontiers in Molecular Biosciences* 3:6.

Nägele T, Mair A, Sun X, Fragner L, Teige M, Weckwerth W. 2014. Solving the differential biochemical Jacobian from metabolomics covariance data. *PLoS One* 9:e92299.

Naikoo MI, Dar MI, Raghib F, Jaleel H, Ahmad B, Raina A, Khan FA, Naushin F. 2019. Chapter 9—role and regulation of plants phenolics in abiotic stress tolerance: an overview. In: Khan MIR, Reddy PS, Ferrante A, Khan NA, eds. *Plant signaling molecules*. Sawston, CA: Woodhead Publishing, 157–168.

Noctor G, Foyer CH. 2000. Homeostasis of adenylate status during photosynthesis in a fluctuating environment. *Journal of Experimental Botany* 51:347–356.

Obata T, Fernie AR. 2012. The use of metabolomics to dissect plant responses to abiotic stresses. *Cellular and Molecular Life Sciences* 69:3225–3243.

Poli R, Kennedy J, Blackwell T. 2007. Particle swarm optimization. *Swarm Intelligence* 1:33–57.

Reznik E, Segrè D. 2010. On the stability of metabolic cycles. *Journal of Theoretical Biology* 266:536–549.

Savitch LV, Barker-Astrom J, Ivanov AG, Hurry V, Oquist G, Huner NP, Gardestrom P. 2001. Cold acclimation of *Arabidopsis thaliana* results in incomplete recovery of photosynthetic capacity, associated with an increased reduction of the chloroplast stroma. *Planta* 214:295–303.

Schaber J, Liebermeister W, Klipp E. 2009. Nested uncertainties in biochemical models. *IET Systems Biology* 3:1–9.

Schulz E, Tohge T, Zuther E, Fernie AR, Hincha DK. 2015. Natural variation in flavonol and anthocyanin metabolism during cold acclimation in *Arabidopsis thaliana* accessions. *Plant, Cell and Environment* 38:1658–1672.

Schulz E, Tohge T, Zuther E, Fernie AR, Hincha DK. 2016. Flavonoids are determinants of freezing tolerance and cold acclimation in *Arabidopsis thaliana*. *Scientific Reports* 6:34027.

Sharkey TD. 1985. Photosynthesis in intact leaves of C_3 plants: physics, physiology and rate limitations. *The Botanical Review* 51:53–105.

Shi Q, Sun H, Timm S, Zhang S, Huang W. 2022. Photorespiration alleviates photoinhibition of photosystem I under fluctuating light in tomato. *Plants* 11:195.

South PF, Cavanagh AP, Liu HW, Ort DR. 2019. Synthetic glycolate metabolism pathways stimulate crop growth and productivity in the field. *Science* 363:eaat9077.

Steuer R, Gross T, Selbig J, Blasius B. 2006. Structural kinetic modeling of metabolic networks. *Proceedings of the National Academy of Sciences of the United States of America* 103:11868–11873.

Strand A, Hurry V, Gustafsson P, Gardeström P. 1997. Development of *Arabidopsis thaliana* leaves at low temperatures releases the suppression of photosynthesis and photosynthetic gene expression despite the accumulation of soluble carbohydrates. *The Plant Journal* 12:605–614.

Strand A, Hurry V, Henkes S, Huner N, Gustafsson P, Gardeström P, Stitt M. 1999. Acclimation of *Arabidopsis* leaves developing at low temperatures. Increasing cytoplasmic volume accompanies increased activities of enzymes in the Calvin cycle and in the sucrose-biosynthesis pathway. *Plant Physiology* 119:1387–1398.

Takahashi S, Bauwe H, Badger M. 2007. Impairment of the photorespiratory pathway accelerates photoinhibition of photosystem II by suppression of repair but not acceleration of damage processes in *Arabidopsis*. *Plant Physiology* 144:487–494.

Tang M, Li B, Zhou X, Bolt T, Li JJ, Cruz N, Gaudinier A, Ngo R, Clark-Wiest C, Kliebenstein DJ, Brady SM. 2021. A genome-scale TF–DNA interaction network of transcriptional regulation of *Arabidopsis* primary and specialized metabolism. *Molecular Systems Biology* 17:e10625.

Warburg O. 1920. Uber die Gesehwindigkeit der photochemichen. *Biochemische Zeitschrift* 103:188–217.

Winkel-Shirley B. 2002. Biosynthesis of flavonoids and effects of stress. *Current Opinion in Plant Biology* 5:218–223.

Wittig U, Rey M, Kania R, Bittkowski M, Shi L, Golebiewski M, Weidemann A, Müller W, Rojas I. 2014. Challenges for an enzymatic reaction kinetics database. *The FEBS Journal* 281:572–582.

Zhang B, Pan C, Feng C, Yan C, Yu Y, Chen Z, Guo C, Wang X. 2022. Role of mitochondrial reactive oxygen species in homeostasis regulation. *Redox Report* 27:45–52.

Zhu X-G, de Sturler E, Long SP. 2007. Optimizing the distribution of resources between enzymes of carbon metabolism can dramatically increase photosynthetic rate: a numerical simulation using an evolutionary algorithm. *Plant Physiology* 145:513–526.